Optimization of cooling strategy and seeding by FBRM analysis of batch crystallization

Dejiang Zhang[a,b], *Lande Liu*[c], *Shijie Xu*[a,b], *Shichao Du*[a,b] ,*Weibing Dong*[a,b], *Junbo Gong*[a,b*]

[a] School of Chemical Engineering and Technology, State Key Laboratory of Chemical Engineering, Tianjin University, Tianjin 300072, People's Republic of China.

[b] The Co-Innovation Center of Chemistry and Chemical Engineering of Tianjin, Tianjin University, Tianjin 300072, People's Republic of China.

[c] School of Applied Sciences, University of Huddersfield, Huddersfield HD1 3DH, UK

ABSTRACT

A method is presented for optimizing the cooling strategy and seed loading simultaneously. Focused beam reflectance measurement (FBRM) was used to determine the approximating optimal cooling profile. Using these results in conjunction with constant growth rate assumption, modified Mullin-Nyvlt trajectory could be calculated. This trajectory could suppress secondary nucleation and has the potential to control product's polymorph distribution. Comparing with linear and two step cooling, modified Mullin-Nyvlt trajectory have a larger size distribution and a better morphology. Based on the calculating results, the optimized seed loading policy was also developed. This policy could be useful for guiding the batch crystallization process.

Keywords: *Batch crystallization; Constant growth rate trajectory; FBRM; Optimized seed policy; Optimization*

1. Introduction

Crystal size distribution is an important quality indicator for particles because it could significantly influence the downstream operation such as filter and drying. Considerable research efforts have been devoted to control the product size distribution.

For optimizing a seeded batch crystallization, generally, it could be divided into two main parts: first, determination of the optimal temperature trajectory; second, optimizing the seed loading policy[1]. Various excellent approaches have been proposed for designing the temperature trajectory or seed loading policy[2-7].

For designing the temperature trajectory, it could be also divided into two main categories, the model-based and model-free approaches[8]. Model-based approaches determine the optimal temperature trajectory by optimizing the crystallization model[9-12]. The widely used crystallization model is the population and mass balance model. Model-free approaches mainly use process analytical technology (PAT) to control the process parameters (such as concentration or particles number) within a certain range which could minimize nucleation[2, 13-17]. In some papers, the boundary of this range is also referred to as secondary nucleation threshold (SNT) [18, 19].

Seed loading is another widely used approach for suppressing nucleation. Kubota and coworkers developed the critical seed loading that is the lowest seed loading ratio for which all of the material crystallizes out of the solution is consumed by the growth of the seeds [20, 21]. Yu-Ti Tseng and Jeffrey D. Ward developed a shortcut approach to determine the seed loading chart and Hsing-Yu Wang and Jeffrey D. Ward applied this approach in the reactive crystallization of barium sulfate and L-glutamic [1, 21].

In this study, we try to find an approach that could optimize the seed loading and temperature trajectory simultaneously. The research published by Kee et al proposed a method that could selective crystallization of metastable α-form L-glutamic [22]. According to their results, the optimized cooling profile was remaining the concentration at a constant relative supersaturation which was the SNT. Using this approach, the FBRM total counts kept constant during the crystallization, hence, secondary nucleation was greatly suppressed. This result was consistent with the conclusion presented by Che-Wei Hsu and Jeffrey D. Ward [6], comparing with analytical trajectory, constant growth rate trajectory have the similar performance of suppressing nucleated mass. Thus, in this study, we will use constant growth rate model to calculate the modified Mullin-Nyvlt trajectory that could desaturate the solution along SNT. According to the characteristic of SNT, when concentration is higher than SNT, contact nucleation or surface breeding would be the dominant nucleation mechanism[18]. Conversely, micro-attrition would be the dominant mechanism. If the cooling trajectory could follow the SNT, this cooling strategy has the potential to control the product size and polymorph distribution simultaneously. In addition, the critical seed loading policy could also be easily calculated by this approach.

2. Method and model

The general idea of this method is to find a cooling profile that could control the solution concentration follows the SNT during the crystallization. Because SNT is generally parallel to solubility, the supersaturation is basically unchanged when cooling

along the SNT, which makes possible to calculate the optimized cooling curve according to constant growth rate model[23]. Therefore, to calculate the modified Mullin-Nyvlt trajectory, the corresponding crystal growth rate at SNT should be determined first.

Theoretically, secondary nucleation threshold could be determined by seeding experiments, as published by Kee et al[22]. However, according to their results, secondary nucleation could not be suppressed when solution concentration followed the limit that was determined by seeded experiments. This may be caused by the surface structure difference between the seeds and the growing crystals[19, 24]. To avoid this deviation, we directly use FBRM to measure at what degree of the cooling rate may lead to nucleation. Using several linear cooling profiles to approximate the optimal cooling profile, and then substitute these linear cooling rate (which were represented by K_1, K_2 and K_3) into model function to calculate the corresponding growth rate. If growth rate is known, the optimized seeding policy and the optimized cooling curve with different seed mass and seed size could also be calculated.

Constant growth rate trajectory could be derived from Mullin-Nývlt's model for the case of no nucleation [12]. If the corresponding crystal growth rate at SNT was represent by g_{max}, all crystals have the same volumetric and surface shape factors, the supersaturation can only be consumed by crystal growth, the general expression of this model is:

$$\frac{-dm_c}{dt} = \frac{-3g_{max}W_s}{L_0^3}(L_t)^2 \quad (1)$$

Where W_S and L_0 are the mass and the size of seeds, respectively; L_t is the crystal

size, m_c is the crystal mass, t is time.

The proposed optimization strategy was used to study the sodium phosphate–water system. This system was chosen because solution is very sensitive to temperature, leading to a low reproducibility. Because there are 12 water molecules in the crystal lattice, we have made a little change to this model.

The mass balance for crystallization were:

$$m_l \cdot c_t + k \cdot m_c = m_0 \cdot c_0 \tag{2}$$

$$m_c + m_l = m_0 \tag{3}$$

Eq. (2) is the solute balance equation and Eq. (3) is the total mass balance equation. m_l is the mother liquid mass, m_0 is the initial solution mass, k is the molecular mass ratio of solute to solvate, e.g. for $Na_3PO_4 \cdot 12H_2O$, k is 0.4316, c_0 is the initial concentration (wt%) of the solute and c_t is solute concentration (wt%) at time t. Solving Eq. (2) and Eq. (3) yields:

$$m_c = \frac{m_0(c_0 - c_t)}{k - c_t} \tag{4}$$

Substituting Eq. (4) into Eq. (1) gives:

$$\frac{dT}{dt} = \frac{-3gw_s(L_t)^2}{m_t L_0^3} \cdot \frac{dT}{d(\frac{c_0 - c_t}{k - c_t})} \tag{5}$$

Since there is no nucleation, the supersaturation is relatively low, c_t can be approximately equal to the solubility c*.

$$\frac{dT}{dt} = \frac{-3g_{max}w_s(L_t)^2}{m_0 L_0^3} \cdot \frac{dT}{d(\frac{c_0 - c^*}{k - c^*})} \tag{6}$$

L_t is derived from the ΔL law:

$$L_t = (\frac{W_p}{W_s})^{\frac{1}{3}} L_0 \tag{7}$$

Where W_P is the total mass of crystals.

$$W_P = W_s + m_c \quad (8)$$

Combining Eqs. (4), (7) and (8) the crystal size L_t can be expressed as:

$$L_t = (1 + \frac{m_0(c_0 - c^*)}{W_s(k - c^*)})^{\frac{1}{3}} \cdot L_0 \quad (9)$$

Substituting Eq. (9) into Eq. (6) gives:

$$\frac{dT}{dt} = \frac{-3g_{max}w_s}{m_0 L_0} \cdot \frac{dT}{d(\frac{c_0 - c^*}{k - c^*})} \cdot (1 + \frac{m_0(c_0 - c^*)}{W_s(k - c^*)})^{\frac{2}{3}} \quad (10)$$

Integrating Eq.5, the optimized cooling curve could be obtained.

3. Experimental Section

3.1 Materials and Apparatus

$Na_3PO_4 \cdot 12H_2O$ (≥ 99% wt, Jiangtian Chemicals Co., Ltd) and deionized water were used to prepare for the solutions. The experiments were performed in a 300mL jacketed crystallizer. Julabo CF41 compatible with Pt100 sensor with ±0.05 K accuracy was used to control the temperature. Mettler FBRM G400 was used to monitor the change of total particle number. Mastersizer 3000 was used to measure size distribution. Olympus MODEL BX53F was used to took the microscopic images of crystals.

3.2 Determine the g_{max}

300g, 43°C saturated sodium phosphate solution was placed in a 400ml jacketed crystallizer. The stirring rate is the same in all experiments, 250rpm/min. The solution was heated to about 50 °C to ensure all crystals had dissolved. The clear solution was then cooled to 43 °C before seeds were loaded. Seed crystals of 206 μm (D50) was introduced into the solution. The amount of seeds used was about 6.5% of the expected yield. The seeded solution was kept at 43 °C for 1h before cooling to polish the crystal surfaces and dissolve the fines. For each experiment, the linear cooling rate was varied

to find the maxima cooling rate under the condition that no nucleation takes place.

Theoretically, the total counts should not change if there is no nucleation. However, attrition and the change of the crystal shape is possible to increase the FBRM total counts[25-27]. Therefore, a criterion should be set to judge whether nucleation took place. A cooling rate of 0.5 °C/h was chosen for this study to determine the effect of attrition and the change of crystal shape on FBRM total counts.

3.3 Comparison and verification experiment

After determined the g_{max}, the optimized cooling curve could be calculated according to Eq.10. Several experiments were carried out to demonstrate the effectiveness of the calculated optimized cooling curve. The initial conditions were same with Section 3.2 except the cooling curve was followed the calculated results. For comparison studies, linear cooling and two steps cooling experiments were also performed. To provide a fair comparison, the total batch time were the same. For linear cooling, the rate is 3.75 °C/h for 5.3 h. For two step cooling, the rate is 2 °C/h for 2 h and then 4.85 °C/h for 3.3 h. The temperature range was from 43°C to 23°C.

Variations in initial seed mass and size were also introduced. The experiments with different seed mass (8g) and seed size (256 um) were also performed.

4. Results and discussion

4.1 The effect of attrition and growth on FBRM total counts

The results of the attrition experiment could be seen in the Fig. 1.

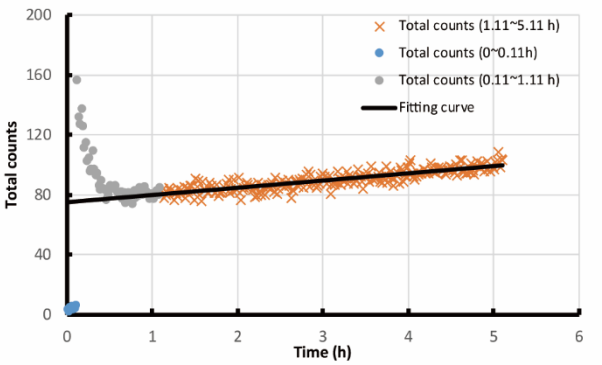

Fig. 1. The FBRM total counts with 0.5 °C/h cooling rate

An increase in the FBRM total counts was observed due to the attrition. Analysis of the total counts show

ed that the effect of attrition on the total counts was linear for the time. The total counts were fit to a linear function:

$$N = 4.859 * t + 74.665 \quad (11)$$

Where *N* is the total counts and *t* (h) is time. The fitting curve as marked by a solid line was showed in Fig .1. The total counts increased 76.366 due to seeding and increased 4.860 due to attrition during 1h. Then, during 1 h, the ratio between 76.366 and 4.860, 6.36%, was used as the criterion to judge whether there is nucleation.

4.2 Determine the approximating optimized cooling rate

Fig. 2 showed the change of total counts with different linear cooling rates in the second hour.

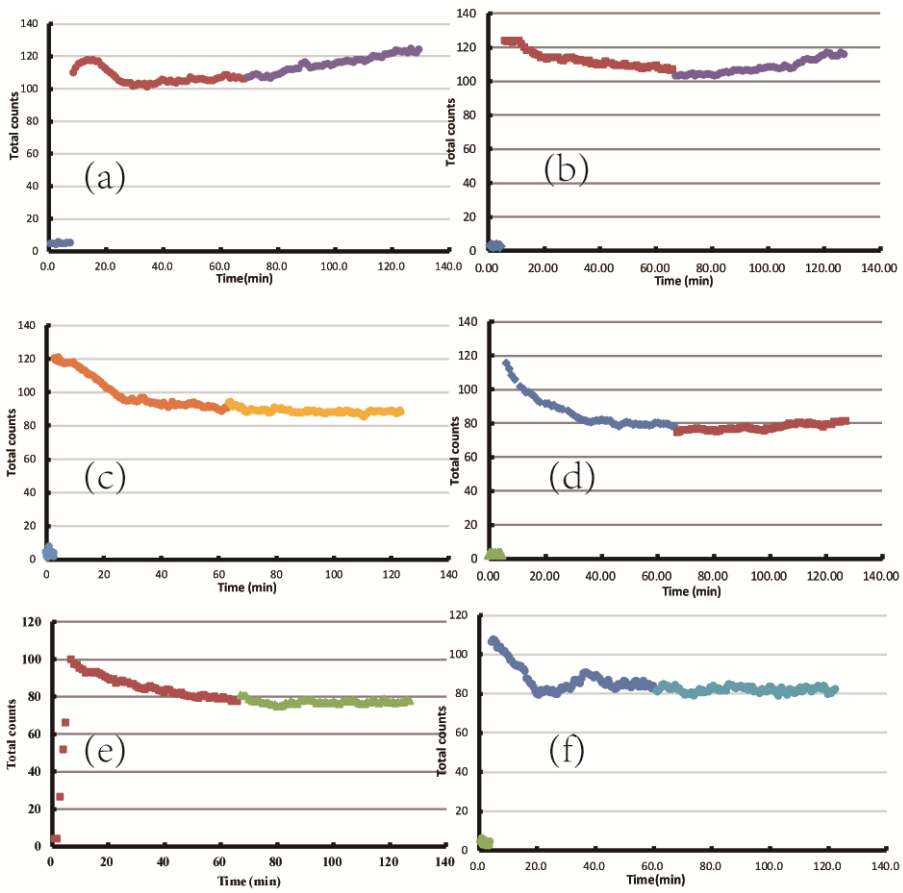

Fig 2. FBRM total counts profile of crystallization with cooling rate of (a) 1.2 °C/h, (b) 1.2 °C/h, (c) 1.0 °C/h, (d) 1.0 °C/h, (e) 0.8, (f) 0.8 °C/h

At the beginning, the number of total counts increased rapidly for the seed loading. Subsequently, it dropped and eventually stabilized at a constant value, which may be due to the effect of Ostwald ripening. The cooling rates were rather small for the second hour because of the relatively small total crystal surface area and sodium phosphate solution tends to precipitate more crystals at high temperature.

As shown in Fig 2, although the initial conditions were the same, the initial total counts of these experiments may not the same, (Run (a) was 111.4 while Run (d) was 75.7). This was caused by the shift of the FBRM probe position in the different batch experiments. Since whether there was nucleation was determined by the changing

percentage of the total counts, the position of the FBRM probe did not affect the results.

To avoid measurement fluctuation, the FBRM total counts were smoothed by Exponentially Weighted Moving-Average (EWMA) algorithm. The weight used for EWMA was 0.3. The change of the total counts could be seen in the Table 1.

Table 1. The change of the FBRM total counts in the first 1 h.

Cooling rates in the first interval (°C/h)	Runs No	Base value	Initial total counts	Endpoint total counts	Change of the total counts	Judging criterion	Suppress nucleation (Y/N)
1.2	a	4.8	107.1	124.3	17.2	6.51	N
1.2	b	3.1	103.5	115.9	12.4	6.39	N
1.0	c	3.4	93.9	88.1	-5.8	5.76	Y
1.0	d	3.1	74.4	81.2	6.8	4.53	N
0.8	e	3.5	80.7	77.9	-2.8	4.91	Y
0.8	f	3.9	81.3	82.2	0.9	4.92	Y

The base value (*BV*) is the background when there are no crystals in the solution. The judging criterion (*JC*) was calculated according to the equation below:

$$JC=(IV-BV)*0.0636 \quad (12)$$

Where *IV* is the initial value and *BV* is the base value. 0.0636 is the increasing percentage caused by attrition.

The effect of cooling rate on the FBRM total counts can be observed, comparing the change of total counts. From run a to f, increased total counts is generally decreased while decreasing cooling rate. For Run e and f, the total counts remained nearly constant, indicating that the solution concentration should below the SNT. At this cooling rate, the growth kinetics were fast enough to desaturate the solution, reducing the

concentration below the SNT. Therefore, secondary nucleation was greatly suppressed. Using a faster cooling rate of 1.2 °C/h, as shown in Runs a and b, a significant increasing in the total counts was observed, implying that secondary nucleation was not will controlled. For the Run c and d, despite the same experimental procedure, it can be observed the variations in the nucleation behaviors. This variation is most likely due to the stochastic nature of nucleation, which is affected by many external factors [28]. At the cooling rate of 1.0 °C/h, the solution concentration should be close to SNT. Hence, the cooling rate of 1.0 °C/h was chosen as the K_1 at 43 °C for the second hour. Although further reduction of the cooling rate could have a better performing in suppressing secondary nucleation, this may lead to a rather long batch times.

Subsequently, kept the cooling rate of 1.0 °C/h for the second hour, the K_2 at 42 °C was also determined. Experimental results in the third hour were showed in Fig. 3.

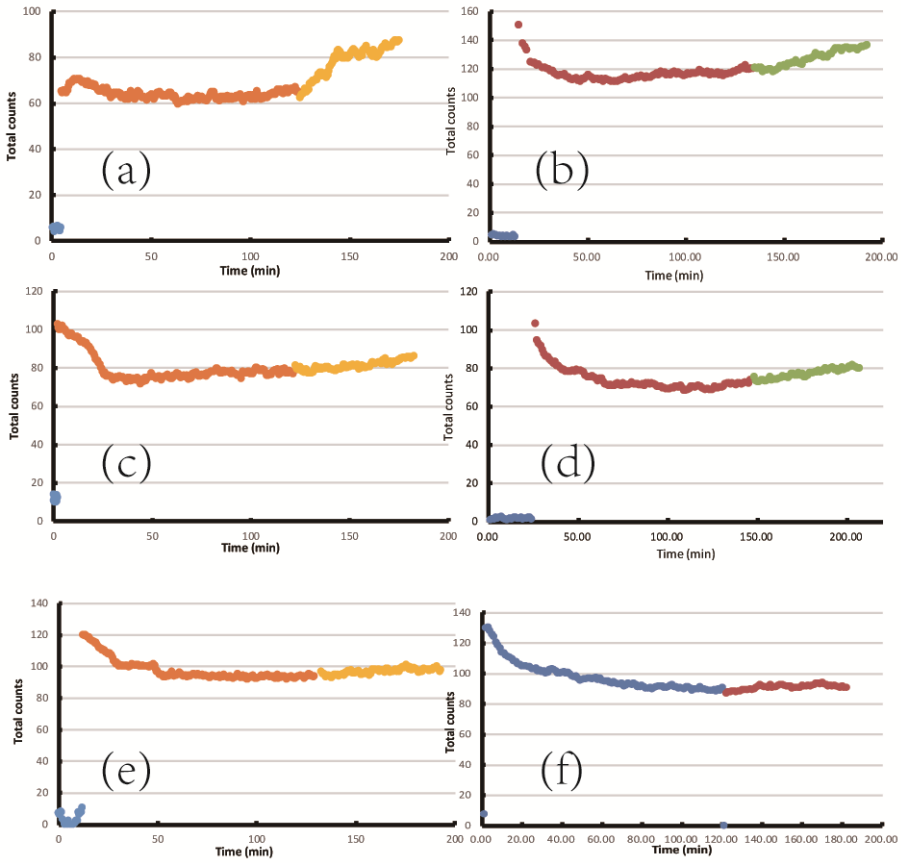

Fig. 3 FBRM total counts profile of crystallization with cooling rate of (a) 2.0 °C/h, (b) 2.0 °C/h, (c) 1.7 °C/h, (d) 1.7 °C/h, (e) 1.5 °C/h, (f) 1.5 °C/h in the third hour

The analysis of the total counts follows the same procedures as described above, the results could be seen in the Table 2.

Table 2. The change of the FBRM total counts in the third hour.

Cooling rates in the first interval (˚C/h)	Runs No	Base value	Initial total counts	Endpoint total counts	Change of the total counts	Judging criterion	Suppress nucleation (Y/N)
2.0	a	5.6	62.6	87.2	24.6	3.63	N
2.0	b	4.1	120.9	136.5	15.6	7.43	N
1.7	c	11.5	81.5	86.2	5.7	4.45	N
1.7	d	1.7	75.4	80.1	4.7	4.69	N
1.5	e	3.5	96.8	97.9	1.1	5.93	Y

1.5	f	7.8	87.0	91.0	4.0	5.03	Y

Based on the result of these experiments, the shift of the dominant crystallization mechanism could be observed at the cooling rate of 1.5 °C/h. At this cooling rate, crystal growth rate outweighs the secondary nucleation rate. In these three experiments, the total counts in the second hour remained nearly constant, which indicates the cooling rate of 1.0 °C/h during the second hour could suppress nucleation.

The same procedures were used to determined K_3 at 40.5 °C. The experimental results were showed in Fig. 4.

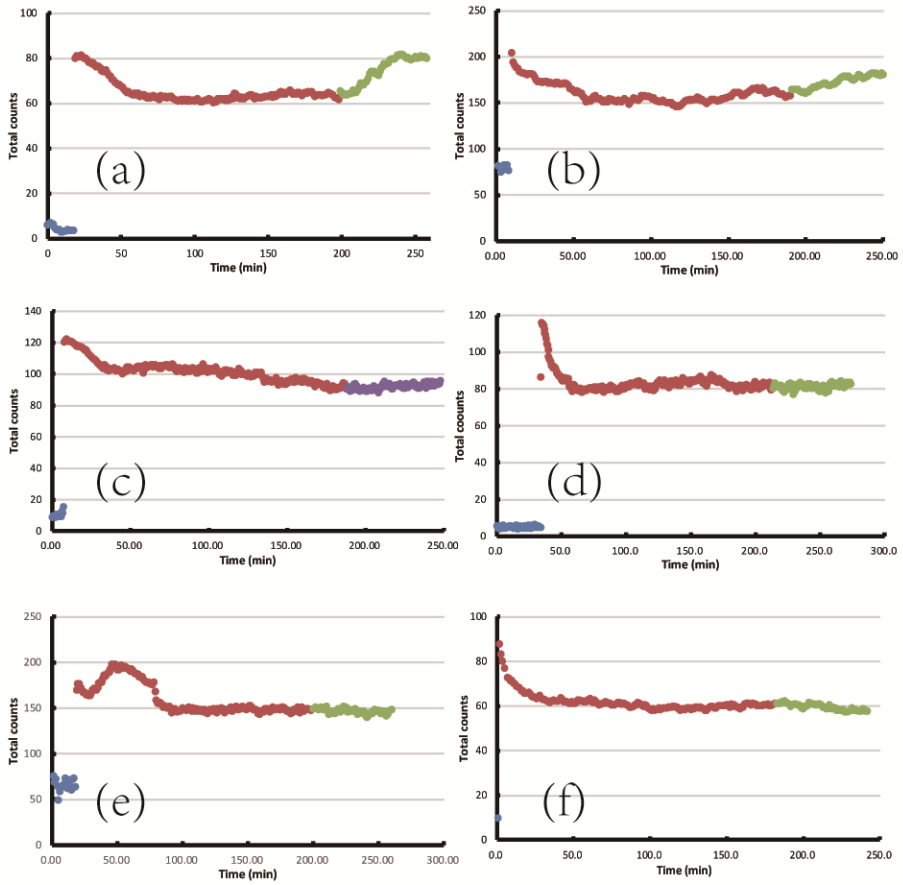

Fig. 4 FBRM total counts profile of crystallization with cooling rate of (a) 2.3 °C/h, (b) 2.3 °C/h, (c) 2.1 °C/h, (d) 2.1 °C/h, (e) 1.9 °C/h, (f) 1.9 °C/h in the fourth hour

Using the same calculating process, the results could be seen in the Table 3.

Table 3. The change of the FBRM total counts in the fourth hour.

Cooling rates in the first interval (°C/h)	Runs No	Base value	Initial total counts	Endpoint total counts	Change of the total counts	Judging criterion	Suppress nucleation (Y/N)
2.3	a	4.3	65.4	79.7	14.3	3.89	N
2.3	b	79.7	164.3	180.5	16.2	5.38	N
2.1	c	10.2	91.0	95.5	4.5	5.14	Y
2.1	d	5.0	80.2	82.6	2.4	4.78	Y
1.9	e	66.4	149.0	148.6	-0.4	5.25	Y
1.9	f	3.3	61.0	56.7	-4.63	3.29	Y

It can be seen from the Table 3, secondary nucleation could be suppressed when the cooling rate down to 2.1 °C/h.

In summary, the approximating optimal cooling curve were 1 °C/h from 43 °C to 42 °C, 1.5 °C/h from 42 °C to 40.5 °C and 2.1 °C/h from 40.5 °C to 38.4 °C.

4.3 Calculate the cooling curves

The solubility of Na_3PO_4 was measured by gravimetric method and fitted by a linear function, the result was:

$$c^* = 0.0032\,T + 0.0442 \qquad (R^2 = 0.9998) \qquad (13)$$

The unit of solubility was wt% (g Na_3PO_4/g solution).

Substituting the experimental results into Eq. (10) and solving it, the growth rate at three different temperature points were:

$$g_1 = 0.0673 \text{ mm/h}, T = 43 \text{ °C} \qquad (14)$$

$$g_2 = 0.0629 \text{ mm/h}, T = 42\ ^\circ\text{C} \quad (15)$$

$$g_3 = 0.0593 \text{ mm/h}, T = 40.5\ ^\circ\text{C} \quad (16)$$

In comparison with the rest growth rate, g_1 was larger. This was because the model assumption that the solution was always have a certain degree of supersaturation, while the above experiments was started at a saturation concentration. Besides, g_2 and g_3 was close, indicating that the assumption that the supersaturation is constant was reasonable. To avoid the deviation, g_1 was deleted. Then, take average of g_2 and g_3 as the g_{max}:

$$g_{max} = 0.0611 \text{ mm/h} \quad (17)$$

In this study, g_{max} was assumed to be constant. However, for the generalized case, it is reasonable to assumed that g_{max} was a function of temperature. Using this growth rate function needs more approximating linear cooling rate, which may be time-consuming. Thus, for the simplification, we would not use the temperature-dependent g_{max} function.

Subsequently, substituting g_{max} into Eq. (10) to calculate the optimized cooling curve. The optimized cooling curve could be seen in Fig. 5.

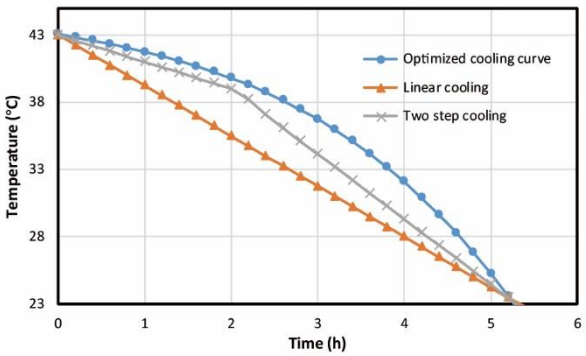

Fig.5 Temperature profile of optimized cooling curve and the comparison cooling curves.

The calculated optimized cooling curve is similar to a cubic trajectory. The slope of the optimized cooling curve was relatively low at the beginning and gradually

increasing through the experiment. That was not only because the total crystal surface was not large enough to rapidly desaturate the solution, but also the fact that the $Na_3PO_4 \cdot 12H_2O$ crystal has 12 water molecules in the lattice, which implies that more crystals tend to precipitate at high temperature.

4.4 Comparison between different cooling strategy

The aim of these experiments was to investigate whether the cooling curve calculated by the g_{max} could suppress the secondary nucleation. Figure 6 showed the profile of temperature and the evolutions of total counts using different cooling strategies.

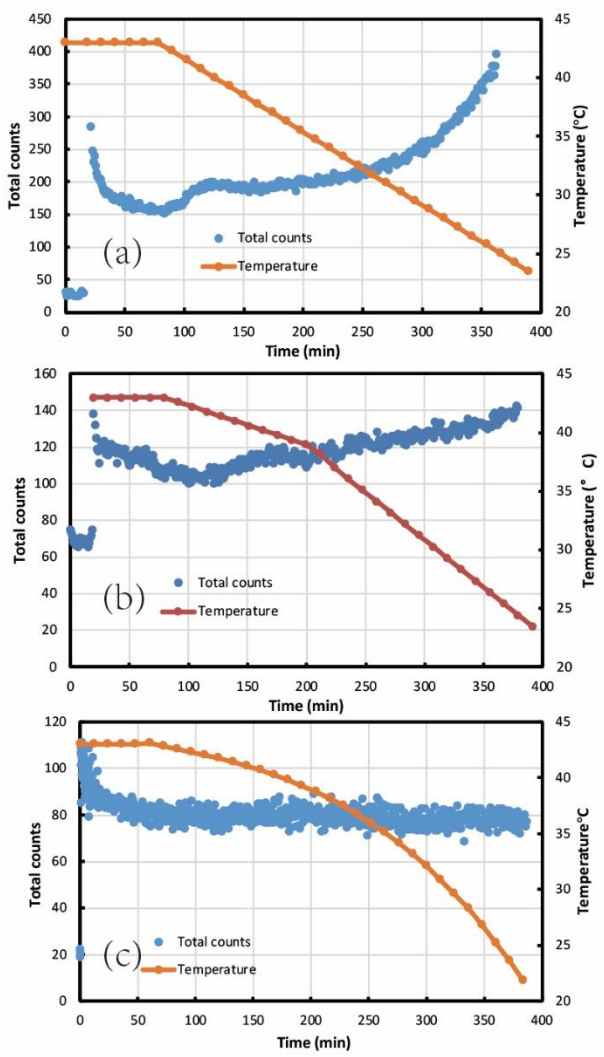

Fig. 6 Temperature and total counts profile of different cooling strategy: (a) linear cooling; (b) two step cooling; (c) optimized cooling

In the case of linear cooling, the strong increase in total counts taken place at the beginning of the cooling period, then the total counts remained constant until 200 min, after 200 min, nucleation continuous increased during the rest process. The similar total counts profile could be observed using two step cooling. Comparing with linear cooling, nucleation was more moderate during two steps cooling. However, distinct increase in the total counts could still be observed using these profiles. While in the optimized cooling run, total counts almost kept constant during the whole process, indicating a better performance in suppressing nucleation.

According to Wang and Ward's conclusion [1, 11], the trajectory that has the constant supersaturation could minimizes the number of nuclei in the case of nucleation was independent of the crystal mass. The result of the optimized cooling curve was consistent with this conclusion because Fig .1 showed that the nucleation rate was relatively independent with the crystal mass.

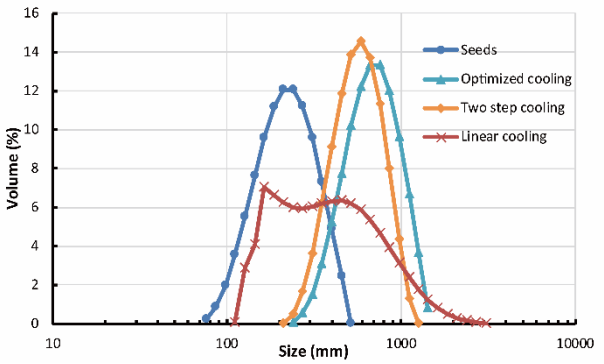

Fig. 7 The size distribution of different cooling strategy

The crystal size distribution (CSD) resulting from three different cooling experiments were showed in Fig. 7. This result confirmed that the modified Mullin-Nyvlt trajectory lead to large crystal size distribution.

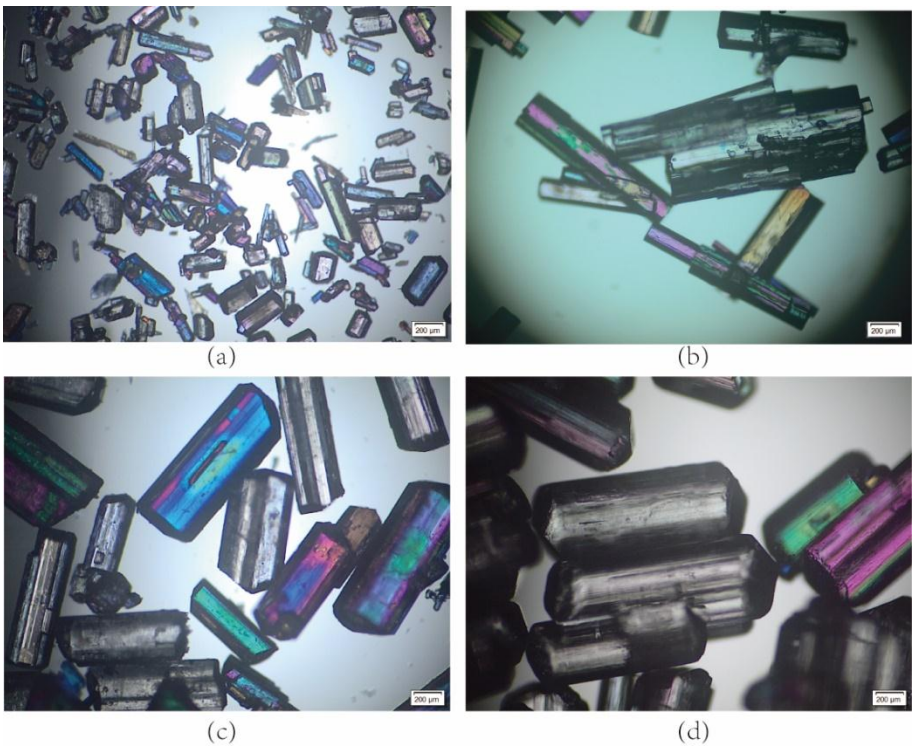

Fig. 8 Microscopic images of (a) seeds, (b) linear cooling product, (c) two step cooling product, (d) optimized cooling product

The microscopy images of different cooling products could be seen in the Fig. 8. All products were inclined to be rod-like shape, while the linear cooling and two step cooling products have a higher aspect ratio. The higher aspect ratio products were more likely break into small fines during the crystallization process. Besides, linear cooling also tends to generate more particles. Therefore, linear cooling products have a wider size distribution.

It is worth noting that although the aspect ratio of seeds and optimized cooling products were similar in this experiment, it is hard to make sure there is no change in the aspect ratio using different seeds. In this model, the shape factor was assumed to be the same during the batch experiment. Therefore, to avoid the deviation, the K_1 was not recommended to use in calculating g_{max}.

4.5 Experiments with different seed conditions

Solving Eq. (10) under different initial seed conditions and using the calculated cooling profile to implement the batch experiments, the results could be seen in the Fig. 9.

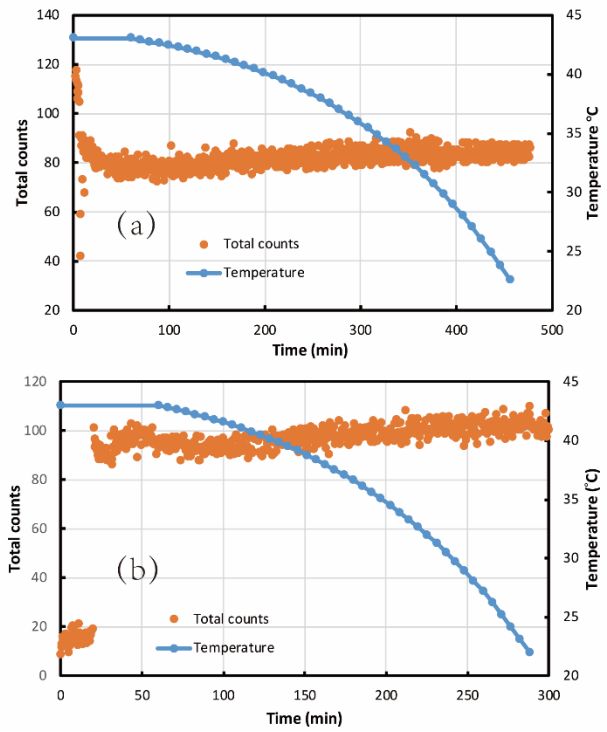

Fig. 9 Optimized temperature and total counts profile of batch experiments with seed size and mass of (a) 0.256 mm and 4 g; (b) 0.206 mm and 8g.

It was found that using this approach, secondary nucleation could also be suppressed under different seed conditions. The total batch time was decreased with the increasing in the seed mass, while the opposite behavior is observed for the increasing the seed size. However, the total batch time was not decreased by two times when doubling the initial seed mass. This was due to the increasing in the total surface area was limit by the mass balance, hence, total surface area was not a linear function of the initial seed mass during the crystallization.

Optimized seed loading policy is a helpful guideline for process design [1]. When g_{max} was known, the optimized seed loading policy could also be developed. In contrary

with the research reported by Tseng and Ward [21], this optimized seed loading policy was prepared only knowing the growth kinetic. For a cooling process that has the certain temperature range, substituting g_{max} into Eq (10), the optimized batch time should be a function of seed size and mass. Plot optimized cooling time against the seed size and mass, the results could be seen in the Fig, (10).

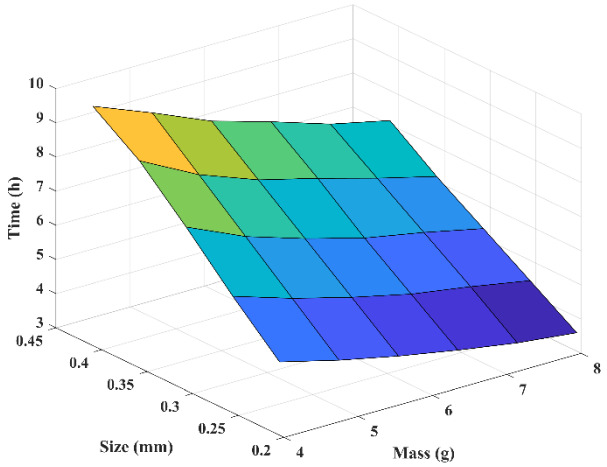

Fig. 10 The optimized seed loading policy.

According to the Fig. 10, the points below this surface would leads to the undesired secondary nucleation even if the cooling profile had been optimized. Comparing with seed mass, seed size has higher impact on the total batch time due to the total surface area is more sensitive to the seed size. However, decreasing total batch time just by decreasing the seed size should be careful because fine seeds tend to dissolve into the solution.

5. Conclusion

In this work, a method is presented for optimize cooling profile and seed loading policy simultaneously. This method directly uses FBRM to determine the approximate linear cooling rate and using these results in conjunction with constant growth rate

model to calculate the modified Mullin-Nyvlt trajectory. The experimental result confirms that the proposed optimizing strategy could effectively suppress secondary nucleation. Comparing with the linear cooling and two steps cooling, optimized cooling product has a larger size distribution and a better morphology. The modified Mullin-Nyvlt trajectory with different seed condition were calculated and its effect on suppressing secondary nucleation was determined. Results showed that these profiles could improve the performance of batch crystallization. Based on the calculating results, the optimized seed loading policy was also developed. This policy could be useful for guiding the batch crystallization process.

Acknowledgements

The authors are grateful to the financial support of National Natural Science Foundation of China (No. NNSFC 21176173 and NNSFC 21376164), National high technology research and development program (863 Program No.2012AA021202), Major Science and Technology Program for Water Pollution Control and Treatment (NO.2015ZX07202-013)

References

[1] H.-Y. Wang, J.D. Ward, Seeding and Optimization of Batch Reactive Crystallization, Industrial & Engineering Chemistry Research, 54 (2015) 9360-9368.

[2] E. Simone, W. Zhang, Z.K. Nagy, Application of Process Analytical Technology-Based Feedback Control Strategies To Improve Purity and Size Distribution in Biopharmaceutical

Crystallization, Crystal Growth & Design, 15 (2015) 2908-2919.

[3] H. Seki, Y. Su, Robust optimal temperature swing operations for size control of seeded batch cooling crystallization, Chemical Engineering Science, 133 (2015) 16-23.

[4] E. Bolaños-Reynoso, K.B. Sánchez-Sánchez, G.R. Urrea-García, L. Ricardez-Sandoval, Dynamic Modeling and Optimization of Batch Crystallization of Sugar Cane under Uncertainty, Industrial & Engineering Chemistry Research, 53 (2014) 13180-13194.

[5] Z.Q. Yu, P.S. Chow, R.B.H. Tan, W.H. Ang, PAT-Enabled Determination of Design Space for Seeded Cooling Crystallization, Organic Process Research & Development, 17 (2013) 549-556.

[6] C.-W. Hsu, J.D. Ward, The best objective function for seeded batch crystallization, AIChE Journal, 59 (2013) 390-398.

[7] A. Fiordalis, C. Georgakis, Data-driven, using design of dynamic experiments, versus model-driven optimization of batch crystallization processes, Journal of Process Control, 23 (2013) 179-188.

[8] E. Aamir, C.D. Rielly, Z.K. Nagy, Experimental Evaluation of the Targeted Direct Design of Temperature Trajectories for Growth-Dominated Crystallization Processes Using an Analytical Crystal Size Distribution Estimator, Industrial & Engineering Chemistry Research, 51 (2012) 16677-16687.

[9] K.L. Choong, R. Smith, Optimization of batch cooling crystallization, Chemical Engineering Science, 59 (2004) 313-327.

[10] Z.K. Nagy, R.D. Braatz, Open-loop and closed-loop robust optimal control of batch processes using distributional and worst-case analysis, Journal of Process Control, 14 (2004)

411-422.

[11] J.D. Ward, D.A. Mellichamp, M.F. Doherty, Choosing an operating policy for seeded batch crystallization, AIChE Journal, 52 (2006) 2046-2054.

[12] J.D. Ward, C.-C. Yu, M.F. Doherty, A new framework and a simpler method for the development of batch crystallization recipes, AIChE Journal, 57 (2011) 606-617.

[13] L.L. Simon, H. Pataki, G. Marosi, F. Meemken, K. Hungerbühler, A. Baiker, S. Tummala, B. Glennon, M. Kuentz, G. Steele, H.J.M. Kramer, J.W. Rydzak, Z. Chen, J. Morris, F. Kjell, R. Singh, R. Gani, K.V. Gernaey, M. Louhi-Kultanen, J. O'Reilly, N. Sandler, O. Antikainen, J. Yliruusi, P. Frohberg, J. Ulrich, R.D. Braatz, T. Leyssens, M. von Stosch, R. Oliveira, R.B.H. Tan, H. Wu, M. Khan, D. O'Grady, A. Pandey, R. Westra, E. Delle-Case, D. Pape, D. Angelosante, Y. Maret, O. Steiger, M. Lenner, K. Abbou-Oucherif, Z.K. Nagy, J.D. Litster, V.K. Kamaraju, M.-S. Chiu, Assessment of Recent Process Analytical Technology (PAT) Trends: A Multiauthor Review, Organic Process Research & Development, 19 (2015) 3-62.

[14] G. Zhou, A. Moment, S. Yaung, A. Cote, T.-E. Hu, Evolution and Application of an Automated Platform for the Development of Crystallization Processes, Organic Process Research & Development, 17 (2013) 1320-1329.

[15] A.N. Saleemi, C.D. Rielly, Z.K. Nagy, Comparative Investigation of Supersaturation and Automated Direct Nucleation Control of Crystal Size Distributions using ATR-UV/vis Spectroscopy and FBRM, Crystal Growth & Design, 12 (2012) 1792-1807.

[16] A. Saleemi, C. Rielly, Z.K. Nagy, Automated direct nucleation control for in situ dynamic fines removal in batch cooling crystallization, CrystEngComm, 14 (2012) 2196.

[17] Z.K. Nagy, R.D. Braatz, Advances and new directions in crystallization control, Annual

review of chemical and biomolecular engineering, 3 (2012) 55-75.

[18] T.L. Threlfall, S.J. Coles, A perspective on the growth-only zone, the secondary nucleation threshold and crystal size distribution in solution crystallisation, CrystEngComm, 18 (2016) 369-378.

[19] S.J. Coles, T.L. Threlfall, A perspective on a century of inert seeds in crystallisation, CrystEngComm, 16 (2014) 4355.

[20] N. Doki, N. Kubota, M. Yokota, A. Chianese, Determination of Critical Seed Loading Ratio for the Production of Crystals of Uni-Modal Size Distribution in Batch Cooling Crystallization of Potassium Alum, Journal of Chemical Engineering of Japan, 35 (2002) 670-676.

[21] Y.-T. Tseng, J.D. Ward, Critical seed loading from nucleation kinetics, AIChE Journal, 60 (2014) 1645-1653.

[22] N.C.S. Kee, R.B.H. Tan, R.D. Braatz, Selective Crystallization of the Metastable α-Form of l-Glutamic Acid using Concentration Feedback Control, Crystal Growth & Design, 9 (2009).

[23] B. Mayrhofer, J. Nývlt, Programmed cooling of batch crystallizers, Chemical Engineering & Processing Process Intensification, 24 (1988) 217-220.

[24] S.S. Kadam, S.A. Kulkarni, R. Coloma Ribera, A.I. Stankiewicz, J.H. ter Horst, H.J.M. Kramer, A new view on the metastable zone width during cooling crystallization, Chemical Engineering Science, 72 (2012) 10-19.

[25] T. Leyssens, C. Baudry, M.L. Escudero Hernandez, Optimization of a Crystallization by Online FBRM Analysis of Needle-Shaped Crystals, Organic Process Research & Development, 15 (2011) 413-426.

[26] I.B. Poblete, C.A. Castor, M. Nele, J.C. Pinto, On-line monitoring of chord distributions in

liquid-liquid dispersions and suspension polymerizations by using the focused beam reflectance measurement technique, Polymer Engineering & Science, 56 (2016) 309-318.

[27] M. Mostafavi, S. Petersen, J. Ulrich, Effect of Particle Shape on Inline Particle Size Measurement Techniques, Chemical Engineering & Technology, 37 (2014) 1721-1728.

[28] M.W. Hermanto, P.S. Chow, R.B.H. Tan, Operating Strategy to Produce Consistent CSD in Combined Antisolvent-Cooling Crystallization Using FBRM, Industrial & Engineering Chemistry Research, 51 (2012) 13773-13783.